Kinematics and timing of polyphase post-Caledonian deformation in the Bergen area, SW Norway

Øystein Larsen, Haakon Fossen, Knut Langeland & Rolf-Birger Pedersen

Larsen, Ø., Fossen, H., Langeland, K. & Pedersen, R.B.: Kinematics and timing of polyphase post-Caledonian deformation in the Bergen area, SW Norway. *Norwegian Journal of Geology*, vol. 83, pp. 149-165. Bergen 2003. ISSN 029-196X.

Polyphase semi-brittle to brittle deformation of the basement rocks of the Øygarden Complex commenced shortly after Caledonian ESE-directed thrusting and followed ductile W-directed shearing. Two main post-Caledonian fracture sets (I and II) are characterized on basis of their geometric relationships, mineral content and deformation styles. An early set of semi-brittle, low-angle faults with E-W to NE-SW trends (Set Ia) is tentatively ascribed to local strain caused by the formation of major E-W trending folds. A more pronounced and regionally more consistent set of NE-SW trending early fractures (Set Ib) formed in response to NW-SE extension and vertical shortening. Sphene in these fractures is dated at around 396 Ma by the U/Pb method. In agreement with field relations and previous work, this age suggests that this portion of the Caledonian orogen cooled from amphibolite facies conditions into the brittle field during the Early Devonian. The age of set I fractures indicates that large-scale, E-W trending folds in the basement are older than similarly oriented folds associated with the Devonian basins of southwest Norway. Later hydrothermal activity along Set 1b fractures is indicated by Rb/Sr two-point mineral dating of epidote and hydrothermally altered alkali-feldspar in the wall rock (363, 369 and 371 Ma). A later phase of brittle deformation involved reactivation of set I fractures and the formation of steep, mainly NNW-SSE trending set II fractures, comprising calcite-filled veins and breccias with minor striated faults. Kinematic analyses indicate that these fractures reflect a change in the extension direction to E-W, possibly around the Devonian-Carboniferous boundary. Set II fractures acted as preferable sites for later reactivation at progressively shallower crustal levels; first by intrusion of Permian dikes and later by the formation of incohesive fault rocks.

Øystein Larsen[1], Haakon Fossen, Knut Langeland & Rolf-Birger Pedersen: Department of Geology, University of Bergen, Allégt. 41, N-5007 Bergen, Norway.
[1] Present address: Statoil, N-5020 Bergen, Norway

Introduction

The post-Caledonian deformation history of the Bergen area (Fig. 1) is known to some extent from unpublished theses (Bernhard 1994; Grünwald 1994; Ytredal 1995), and has recently been summarized by Fossen et al. (1997) and Fossen (1998) on the basis of new data. Somewhat simplified, this deformation history has been considered in terms of four regionally significant tectonic phases (Fig. 2). The *first phase* involved heterogeneous top-to-the-W ductile shearing, as described by Fossen & Rykkelid (1990) and Rykkelid & Fossen (1992). Late structures formed during the shearing show evidence of semi-ductile conditions, consistent with syn-kinematic cooling. In particular, the late shearing is characterized by brittle deformation of competent layers in otherwise ductilely deformed rocks. During the *second phase*, these ductile to semi-ductile structures were cut by brittle faults that conform with NW-SE directed crustal extension (Fossen 1998, this study), consistent with the regional strain field as inferred from other parts of southwest Norway (Seranne & Seguret 1987; Fossen 1992; Valle 1998; Osmundsen et al. 1998; Odling & Larsen 2000). The *third phase* caused opening of coast-parallel fractures and the injection of dikes during the E-W directed Permian extension (Løvlie & Mitchell 1982; Fossen 1998). Permo-Triassic dikes of the same kinematic significance are well known along the coast of southwest Norway to the south of Bergen (Færseth et al. 1976; Fossen & Dunlap 1999) and also to the north of Bergen (Torsvik et al. 1997). Thus, these dikes reflect a regionally consistent shift in the extension direction. Finally, the fourth phase, probably consisting of several events (not shown on Fig. 2), involved late- to post-Jurassic reactivation of pre-existing structures and the formation of incohesive fault rocks at shallow crustal levels (Fossen et al. 1997). The latter two phases are generally ascribed to rifting in the North Sea, which in broad terms consists of Permo-Triassic and late Jurassic-early Cretaceous rifting (e.g. Gabrielsen et al 1990).

This paper presents new data from the basement area west of Bergen that contribute to a better understanding of the deformation history briefly outlined above. In particular, we present U/Pb and Rb/Sr dating of minerals related to post-Caledonian fractures that confine the second main deformation phase to the Devonian. Previous timing of this phase was limited to early Devonian $^{40}Ar/^{39}Ar$ cooling ages from the gneisses

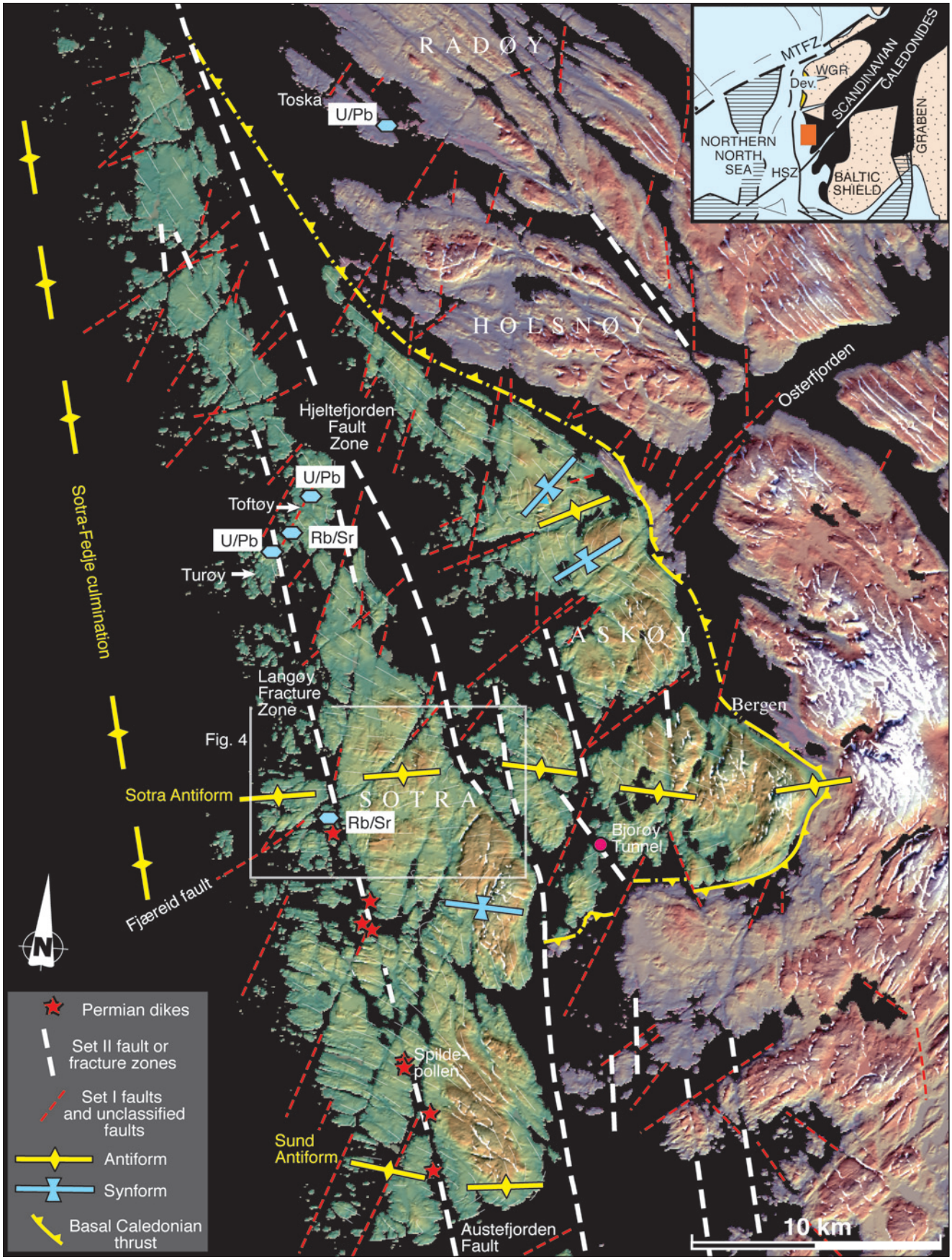

Fig. 1. Shaded digital elevation model of the western Bergen Arcs System with main structures indicated. The basement area in the west and the Caledonian nappe area to the east are given different color values and are separated by a "basal Caledonian thrust". Sampling locations for U/Pb and Rb/Sr dating are shown. Index-map abbreviations: WGR=Western Gneiss Region, MTFZ=Møre-Trøndelag Fault Zone, Dev.=Devonian basins.

(Boundy et al. 1996; Fossen & Dunlap 1998; Fossen 1998), which provide a maximum age for the early fracturing. In addition, field relations and kinematic analyses in this study indicate that the change in extension direction from NW-SE to E-W took place prior to the intrusion of Permian dikes.

Geological framework

The Bergen Arc System (Kolderup & Kolderup 1940) comprises a sequence of Caledonian nappe complexes with contrasting lithologies and metamorphic histories (Sturt & Thon 1978) (Fig. 1), as well as an underlying basement complex. The present fieldwork is carried out in the basement complex named the Øygarden Complex (ØC), which represents the parautochthonous basement onto which these nappes moved eastward during the Caledonian orogeny. The nappe transport was completed in the Early Devonian, and Middle Devonian molasse sediments were deposited in the northernmost part of the Bergen Arc System at the top of the eroded nappe stack, as well as further north in large, tectonically controlled basins (Steel et al. 1985). In the Bergen area, the Devonian deposition was related to oblique/normal displacement along the Bergen Arc Shear Zone, which juxtaposes the Bergen arcs against basement rocks of the WGR to the east (Fossen 1992; Wennberg & Milnes 1994; Wennberg et al. 1998).

Most of the ØC consists of felsic gneisses formed by ductile reworking of Precambrian migmatites and granites (Sturt et al. 1975; Johns 1981; Bering 1984; Fossen & Rykkelid 1990). They show a pervasive S/L fabric, mainly due to i) Caledonian E-directed thrusting and ii) ductile W-directed reversal of this nappe transport. The fabric generally comprises an E-dipping foliation with an E-plunging stretching lineation, reflecting the position of the ØC on the eastern limb of a broad N-S trending antiformal structure, the Sotra-Fedje culmination (Fig. 1, Larsen 1996; Milnes & Wennberg 1997). However, major E-W trending folds, such as the upright Sotra and Sund antiforms, locally disturb this general attitude of the gneiss fabric. The formation of the Sotra-Fedje Culmination and the E-W trending folds affected the overlying Caledonian nappes, indicating that they formed after the nappe emplacement.

Non-coaxial deformation with abundant top-to-the-W kinematic indicators is recognized in high-strain zones throughout the ØC (Fossen & Rykkelid 1990; Rykkelid & Fossen 1992). Kinematic indicators include asymmetric boudins, shear bands, reverse slip crenulations, asymmetric quartz shape fabrics, and asymmetric mica fish and foliation boudinage. Amphibolite facies fabrics are common, but are in places replaced by greenschist-facies composite fabrics where brittle and ductile struc-

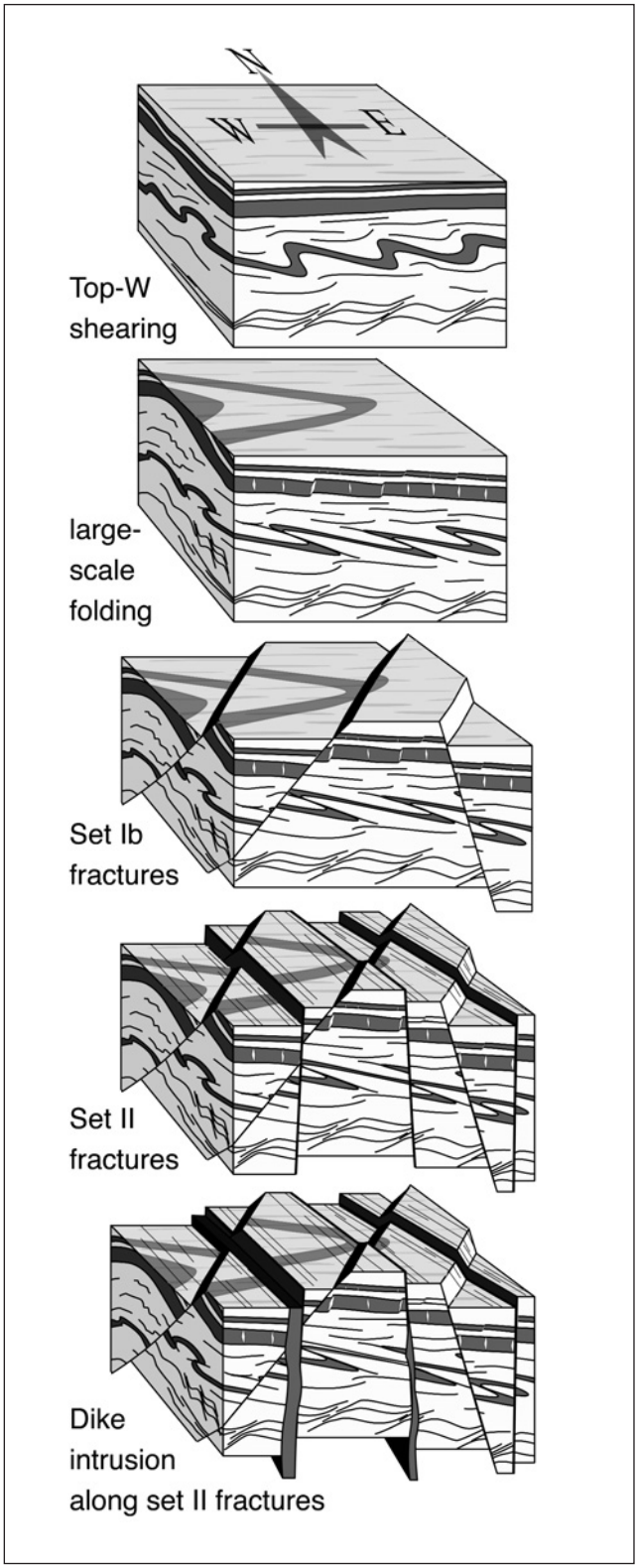

Fig. 2. Illustration of the general tectonic development of the ØC. The formation of the two sets of fractures discussed in the text (set I and II) is shown. The first phase involved ductile to semi-ductile deformation related to W-directed, non-coaxial shearing. The illustration shows the development from ductile, W-directed Early Devonian shearing via the formation of roughly E-W trending macro-scale folds to the development of set I and II fractures and Permian dike intrusion. Subsequent reactivation, with the formation of incohesive fault rocks at shallow crustal levels, is not shown.

tures coexist. The brittle structures are tension cracks and shear fractures confined to competent granitic and amphibolitic layers, whereas surrounding biotite-rich layers only show evidence of ductile flow. Field relations clearly show that such brittle and ductile structures developed simultaneously for a while (Fig. 3), indicating that the rock at the time was entering the brittle-plastic transition in the crust. Evidence for rapid cooling is provided by $^{40}Ar/^{39}Ar$ dating, where amphiboles from the amphibolite-facies fabrics yield ages around 410 Ma (cooling through 500-550°C), whereas biotite yield ages of around 400 Ma (cooling through 300-350 °C) (Boundy et al. 1996; Fossen & Dunlap 1998). A somewhat earlier amphibolite-facies mineral assemblage indicates temperatures of around 670°C (Boundy et al. 1996).

Fig. 3. Set I fracture, Turøy. The epidote-filled fracture is confined to a granitic layer in banded gneiss, suggesting that the temperature was low enough for brittle deformation to occur in this layer, but not in the adjacent mica-bearing layers. Note ductile bending of the gray layer at its lower termination and hydrothermal alteration of the host rock around the fracture. Coin for scale is 2 cm.

Brittle structures on Sotra

Large-scale structures

The ductile-brittle structures described above are overprinted by several sets of brittle fractures. Here we describe their orientations, kinematics, mineral fills and crosscutting relations. Field studies of the fractures have been focused on the Langøy-Algrøy area on Sotra (Fig. 4). In this area, the NE-SW trending *Fjæreid fault* and the NNW-SSE trending *Langøy fracture zones* represent long-lived deformation zones that give a representative picture of the brittle, post-Caledonian deformation history of the ØC.

The Fjæreid fault is a pronounced structure that belongs to a population of roughly NE-SW trending lineaments cutting the E-W trending folds in the ØC (Fig. 1). The structure can be traced some 10 km across Sotra, and may represent a segment of a larger lineament that crosscuts the entire Bergen Arc System along the trend of Osterfjorden (Fig. 1).The Fjæreid fault appears to be a steep structure, and several joints in the fault damage zone exhibit subvertical orientations. The subvertical joints may, however, be late features, and epidote-bearing faults within the fault zone, dipping approximately 60-70° SE, are more likely to reflect the initial orientation of the Fjæreid fault. Geologic mapping by Johns (1981) shows a pattern of lithological mismatches, consistent with sinistral and/or reverse faulting (Fig. 4). Kinematic observations of minor faults along the Fjæreid fault indicate normal dip-slip to strike-slip displacement, thus, a reverse displacement is considered unlikely. No displacement of the Sotra antiform is evident from the bedrock map (Johns 1981), probably because the hinge region is broad and poorly defined in this area.

The NNW-SSE trending *Langøy fracture zone* represents another prominent lineament trend in the Bergen area (Fig. 1). The orientation of subordinate fractures suggests that the fracture zone is a steep or vertical structure. A brief inspection on Algrøy (Fig. 4) indicates that no significant (km-scale) lateral displacement of the Sotra antiform hinge region occurred, but some dip-slip displacement may have occurred. Subordinate structures along the fracture zone comprise both striated faults and, more commonly, hydrofractures (veins) with no detectable fracture-parallel displacement. This predominant dilational deformation and lack of indicators of significant displacements, is taken to suggest an overall joint-dominated (mode I) evolution, with subordinate faulting occurring within the fracture zone. The southward continuation of the Langøy fracture zone, however, appears to be a fault (the Austefjord fault) as indicated by lithologic mismatches (Bering 1984; Fossen 1998). A number of basaltic dikes of Permian age (Løvlie & Mitchell 1982) are localized along the Langøy fracture zone/Austefjord fault (Fig. 4), and the similarity with mantle-sourced dikes of Permian and Triassic age to the south (Færseth 1978) suggests crustal-scale deformation.

Another prominent NNW-SSE trending lineament is the *Hjeltefjord fault zone*, which juxtaposes tectonostratigraphically high nappe units in the Bergen Arc System in the east with gneisses of the ØC in the west (Fig. 1, Fossen 1998). Along one of the faults associated with this fault zone, late Jurassic sediments (the Bjorøy Formation) were discovered during construction of a subsea tunnel, and hence documenting that the fault zone was active both prior to and after deposition of the Jurassic sediments (Fossen et al. 1997).

It will be shown below that epidote and calcite precipitated along the fractures described above at different times. Calcite is the youngest mineral phase, and preci-

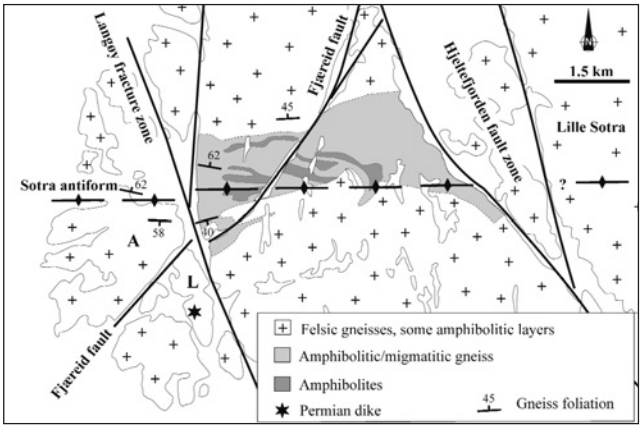

Fig. 4. Simplified geological map of central parts of Sotra (modified from Johns, 1981). The fieldwork was mainly carried out around the intersection between the Fjæreid fault and Langøy fracture zone. A: Algrøy, L: Langøy. See Fig. 1 for location.

pitated on fractures related to the NNW-SSE trending Langøy fracture zone. Furthermore, pre-existing epidote-filled fractures related to the NE-SW trending Fjæreid fault were reactivated and re-mineralized with calcite at this stage. The following classification and characterization of the fracture sets is therefore in part based on their mineral content.

Epidote-mineralized fractures (set I)

Epidote-filled fractures with epidote are here referred to as set I fractures (Table 1). Epidote is commonly present in semi-brittle to brittle extensional faults and veins with trends that range between E-W to NNW-SSE (Fig. 5). We have separated the epidote-bearing fractures into two subsets (a and b) based on orientation, kinematics, and ductility. The two subsets generally show the same fracture-filling minerals, which besides epidote comprise quartz, chlorite and occasional sphene crystals (Fig. 6a). Calcite also occurs, but relates to later reactivation. Set I fractures are characteristically associated with marked hydrothermal alteration, caused by fluids permeating the nearest wall rock. The alteration appears as reddish or pale zones along the fractures, in distinct contrast to the surrounding gneiss (Fig. 3 & 6b). In thin section, these cm- to dm-wide zones of alteration can be seen to affect the feldspars in the gneiss (mostly alkali-feldspar), resulting in a brownish and cloudy appearance (Fig. 6c). The feldspars contain tiny inclusions with optical characteristics consistent with sericite, typically produced from the action of hydrothermal solutions (Deer at al. 1992).

Set Ia faults. – The epidote-bearing fractures of this sub-population differ from most set I fractures by their ductile deformation component and lower dip-angles. Ductile deflection of the gneiss fabric consistent with normal displacement (Fig. 6d) is characteristic of set Ia fractures, indicating that they represent relatively deep (early) structures.

The gneiss foliation around some set 1a faults, preferably those with mica-rich surfaces, is polished with striations that plunge more to the south than the older E-plunging stretching lineation. Thus, it is likely that the

Table 1. The main fracture sets are their characteristics

	Set 1a	Set Ib	Set II
TREND	Variable	NE-SW	N(NW)-S(SE)
FAULT ROCKS	Semi-brittle	Brittle, cohesive, green	Calcite breccias
DOMINANT TYPE OF FRACTURE	Shear fractures (faults)	Shear fractures	Tension fractures
MINERALS	Epidote, quartz, chlorite, sphene, white mica, biotite + secondary calcite	Epidote, quartz, chlorite, sphene + secondary calcite	Calcite, quartz, chlorite.
SIDEWALL	Marked K-spar	Marked K-spar	No marked
ALTERATION	alteration	alteration	alteration
STRIATIONS	Mostly dip slip (normal)	Dip slip (normal), some strike slip	Dip slip to strike slip.
KINEMATICS	WNW-ESE	NW-SE extension	E-W extension
GEOCHRONOLOGY		399-393 Ma (U/Pb) 371-363 Ma (Rb/Sr)	

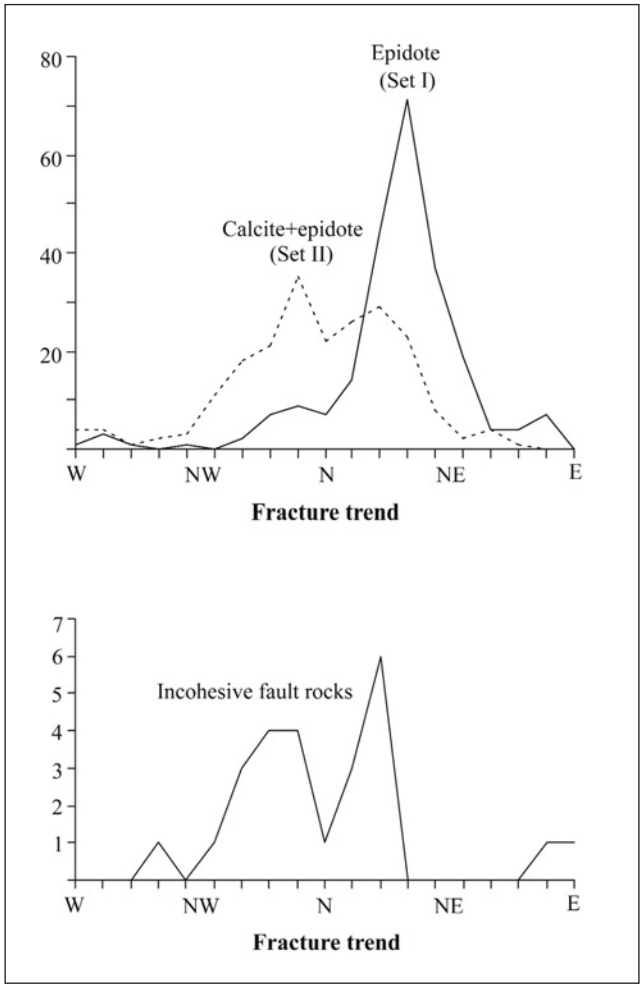

Fig. 5. Frequency diagrams showing trends of set I and set II fractures and fractures with incohesive fault rocks. Note how calcite-filled fractures (set I+II) overlap with epidote fractures (set I). The data are mainly from the area where the Fjæreid fault and Langøy fracture zone intersect (Fig. 4).

foliation was locally reactivated in cases where the orientation was suitable. Multiple set Ia faults occur along the margins of the Fjæreid fault, to which they are subparallel (Fig. 6d). Elsewhere they show orientations that seem to be related to their position on the Sotra and Sund antiforms (Fig. 7). In the Langøy-Algrøy area, which is situated at the southern limb of the Sotra antiform, set Ia fractures strike E-W to ENE-WSW with southerly dips. Low-angle faults with opposite dip directions are occasionally seen further south on Sotra, in an area situated at the northern limb of the Sund antiform (Fig. 1). The extensional nature of these faults implies that the local displacement direction was away from the hinge region of the antiforms, toward the synform lying in between. In the area between the two antiforms, where the folding did not affect the east-dipping foliation much, set Ia faults strike around N-S to NE-SW with both easterly and westerly dips (Fig. 7). Striations seen here are consistent with top-to-the-WNW and ESE displacements. The faults in the latter area often contain coarse-grained white mica and biotite in addition to the epidote-quartz-chlorite mineral assemblage, suggesting deformation under greenschist facies metamorphism. The spatial relationship between set Ia faults and the E-W trending folds is tentatively taken to reflect local strain conditions around the folds.

Set Ib faults. – The main population of epidot-bearing fractures (set Ib) predominantly strikes NE-SW to NNE-SSW (Fig. 5). Set Ib fractures do not show mesoscopically visible ductile wall rock deformation, nor do they exhibit a relationship with the macroscopic folds. They transect all ductile structures throughout the Sotra-Øygarden area, where they reach lengths of several kilometers (Fig. 1). In the Langøy-Algrøy area, set Ib fractures occur in association with the Fjæreid fault, to which they probably are related. However, epidote is also found along a small group of NNW-SSE trending fractures along the Langøy fracture zone in addition to calcite (see below), suggesting that the Langøy fracture zone was an active structure already at the time of epidote deposition.

Set Ib fractures comprise both extensional veins with little or no displacement as well as faults with polished and well-striated surfaces. The faults generally exhibit normal-sense displacement with a minor component of dextral slip (Fig. 8). A less common striation trend on the epidote-coated shear fractures is consistent with strike-slip dominated displacement. Both striation trends may occur on the same fault surface, indicating that some of the set Ia fractures were reactivated, probably under different stress conditions. Occasionally, mineralized steps at fault surfaces show that the strike-slip dominated faults are sinistral, in agreement with several observations of right-stepping *en echelon* fracture arrays associated with these faults (Riedel shears).

Various crush breccias and cataclasites characterize the deformation along many set I faults. These fault rocks often comprise fine-grained epidote-group minerals with a pale greenish appearance in hand specimen. In thin section, the fault-related fabric can be seen to have evolved through alternating episodes of deformation and epidote precipitation, typical for hydrofracturing. The extensional veins, in contrast to the faults, are normally filled with relatively coarse-grained, sometimes euhedral epidote with a bright appearance. In some faults, both fine- and coarse-grained epidote occur, whereas other fault segments are apparently unmineralized. These differences could be the result of displacement along irregular fault surfaces or releasing steps, causing epidote to be deposited preferentially in opening segments of the non-planar fault surfaces. Calcite is often associated with set I fractures. However, microscale crosscutting relationships in these fractures always show that calcite precipitated at a later stage than epidote.

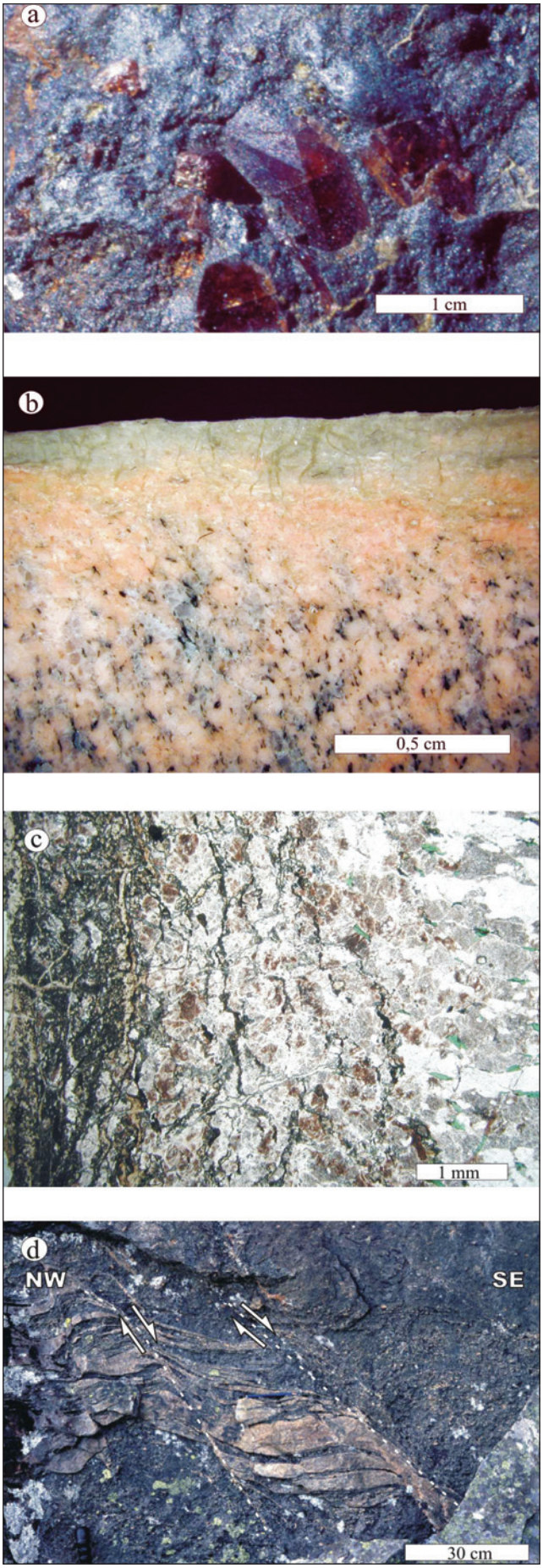

Calcite-mineralized fractures (set II)

Calcite occurs in all fracture sets, many of which also contain epidote (Fig. 5). However, a large number of calcite-filled fractures without epidote are oriented between N-S and NW-SE. These fractures, hereafter referred to as set II, are most abundant along the Langøy fracture zone and other minor fracture zones with similar orientations. Their formation therefore reflects an important phase in the evolution of the NNW-SSE trending lineaments in the ØC. Hydrothermal alteration of the wall rock is generally absent, except for rare cases where epidote also occurs (interpreted as reactivated set I fractures). Since such alteration is generally enhanced by elevated temperatures (Evans 1993), the absence of wall rock alteration is taken to indicate a lower temperature during calcite precipitation than during the formation of set I fractures.

Generally, the formation of set II fractures involved dilation with little or no shearing. Most fractures appear as veins with coarse-grained, euhedral calcite, indicating that the minerals precipitated in open voids. Some set II fractures comprise breccia veins up to several tens of cm's wide (Fig. 9a). Angular rock fragments "floating" in a matrix of hydrothermal calcite characterize these breccia veins. Two main fragment types can be distinguished from thin section study. The most common type corresponds to the surrounding wall rock; the other makes up mm-scale elongated fragments that contain very fine-grained ultracataclasites dominated by quartz matrix (Fig. 9b). In general, the ratio between the hydrothermal calcite matrix and fragments is relatively high, and the fragments occur isolated from each other. This suggests that the brecciation process did not involve significant shear-related fracturing of the wall rock. Phillips (1972) describe a brecciation process in which the sudden stress release associated with hydraulic fracturing causes the wall rock to burst apart as high-pressure fluids enter the fracture. A process like this, without significant shearing, is thought to be responsible for the formation of the hydrothermal breccia veins in the ØC.

Although most set II fractures are dilational by nature, exceptions are represented by faults with slickensides and evidence of cataclastic deformation. The striations

Fig. 6. (a) Euhedral sphene crystal associated with chlorite and epidote on a set I fault near Turøy (Fig. 1). (b) Polished hand sample showing an epidotized set I fault surface (top) with a few millimetres thick zone of hydrothermally altered wall rock. The sample is from the Turøy area and corresponds to sample EP1 dated by the Rb/Sr method. (c) Microphotograph (plane polarized light) of the same sample as shown in (b); epidotized fault surface to the left, altered wall rock in the centre and unaltered wall rock to the right. (d) Normal set Ia faults with ductile deflection of the gneiss foliation from the southern margin of the Fjæreid fault.

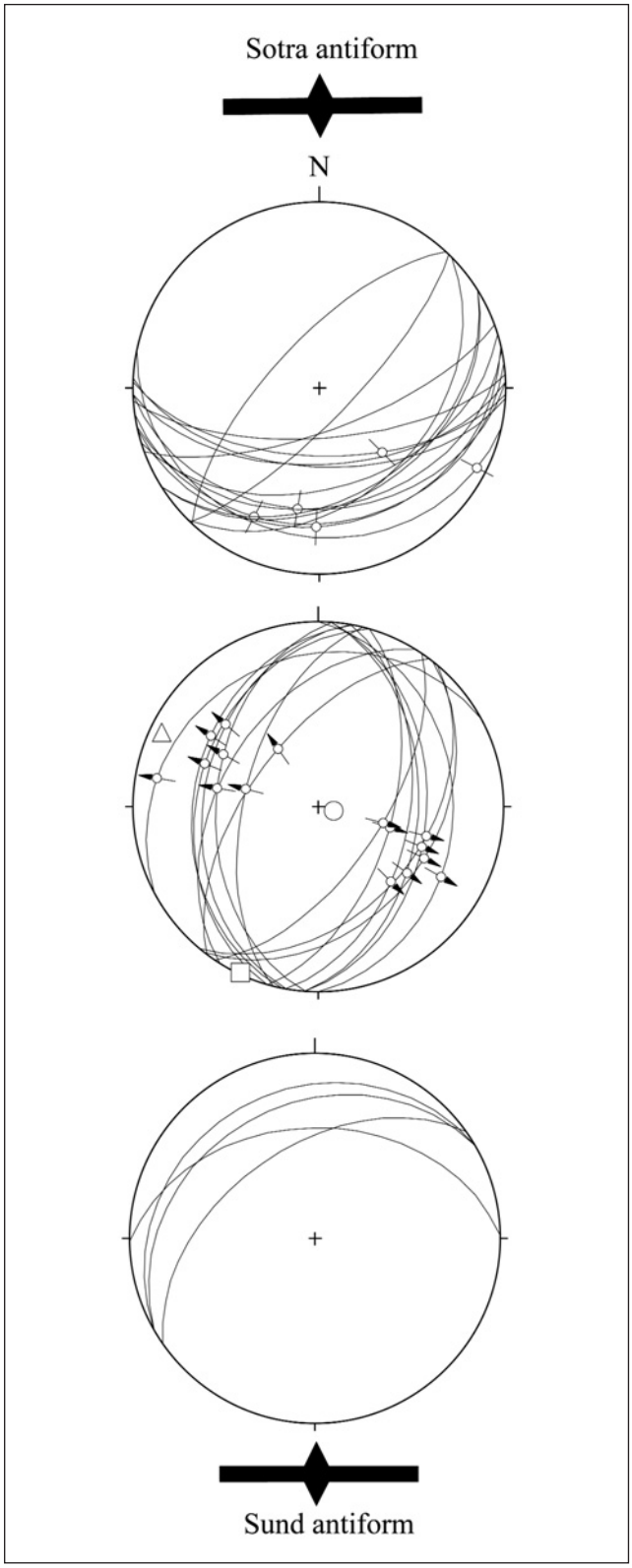

Fig. 7. Stereoplots (equal area lower hemisphere projections) of set Ia fractures from different locations relative to the Sotra and Sund antiforms (Fig. 1). The upper and lower plots are from the southern limb of the Sotra antiform and the northern limb of the Sund antiform, respectively. The middle plot represents the area between the antiforms. The circle, square and triangle refer to the principal stress axes σ_1, σ_2 and σ_3, respectively, inferred from inversion analysis (see also Fig. 10). Striations are indicated, and arrows show observed slip directions.

on these faults, occasionally developed in calcite, range from dip-slip to strike-slip. However, in contrast to set I faults, the displacement is generally strike-slip dominated (Fig. 8). Occasionally, steps at fault surfaces and consistently right-stepping en echelon geometries (Riedel shears) indicate sinistral slip on N-S trending fractures (Fig. 9c). Within the Fjæreid fault, oblique sinistral reactivation of NE-SW trending set I fractures with calcite is also indicated by this type of criterion.

Along some set II faults, the deformation differs in style across distinct mm-scale zones, consistent with a multistage development (Fig. 9d). For instance, deformed calcite along some of the faults is cut by undeformed calcite veins. Slickensides appear as 1-2 mm thick ultracataclasite zones with a random or foliated matrix, both dominated by very fine-grained quartz with minor amounts of sericite or clay minerals. The foliated fabric is characterized by microscopic, anastomosing shear bands that contain elongated quartz with strong lattice-preferred orientation (Fig. 9e). Thus, the slickensides appear to be influenced by crystal-plastic mechanisms (e.g. Passchier & Trouw 1996). However, the deformation related to these faults was primarily associated with cataclasis and produced very low-grade mineral assemblages (sericite and/or clay minerals), indicating that bulk rock temperatures were below that of the crystal-plastic deformation regime of quartz. Some of the fragments in the hydrothermal breccia veins described above (Fig. 9b) are thought to be remnants of the slickensided surfaces. Thus, all together, these observations indicate a multi-stage development of set II fractures that generally involved early faulting and later hydraulic brecciation.

Incohesive fault rocks

Incohesive fault rocks, mostly fault gouge, are observed in fracture zones that follow the main trends described above. In particular, fractures with trends around N-S are commonly recorded with fault gouge (Fig. 5). In addition, steep fault gouge zones with NW-SE trend were observed during operations in the Bjorøy tunnel (Fig. 1, Fossen et al. 1997). These shallow fault rocks are apparently not associated with mineral precipitation. Rather, deformed remnants of calcite veins occur in the fault gouge. Striations on these late fractures are rare and faint.

Relative age relationships

Microscale crosscutting relationships consistently show that epidote precipitated prior to calcite. The record of brittle fracture trends and related mineralization (Fig. 5) provides further information on the relative age of the two prominent NE-SW and NNW-SSE fracture trends in the ØC. Epidote is predominantly confined to

fractures trending NE-SW to NNE-SSW (set Ib). Calcite, on the other hand, occurs on fractures of any trend, including those with epidote (sets I+II). In other words, when epidote precipitated, the only fractures accessible for circulating fluids were generally those related to set I. Calcite precipitated during later deformation when a wider range of fracture trends was available for precipitation, that is, when set II fractures formed as a multistage response to the evolution of the Langøy fracture zone. Thus, the calcite precipitation involved formation of new fractures with trends ranging from N-S to NW-SE, as well as reactivation of pre-existing set I fractures.

The formation of striated set II faults apparently preceded the hydraulic brecciation, since ultracataclasites from these faults are found as fragments in the breccia veins. The Permian (260 Ma) dikes are generally undeformed or weakly deformed, even where they intrude zones of intense deformation (Fossen 1998). Minor veins and faults with calcite have been seen to affect one of these dikes in Spildepollen (Fig. 1), suggesting that some set II fractures formed coevally with the dike intrusion. Thus, the Permian dikes were likely intruding during or following the latest stages in the formation of set II fractures.

The latest identified phase(s) in the structural evolution of the ØC involved reactivation of pre-existing fractures and formation of incohesive fault rocks, containing remnants of deformed calcite veins. The incohesive nature of these fault rocks indicates reactivation at shallow crustal levels. Such faults are shown to affect Late Jurassic (Oxfordian) sediments of the Bjorøy Formation (Fossen et al. 1997), indicating that at least some faulting is latest Jurassic or younger in age.

Kinematic analysis

The direction of principal paleostress axes in brittlely deformed areas can be inferred by direct inversion analysis of fault-slip data (e.g. Angelier 1984; Etchecopar et al. 1981). Parameters included in such analyses are the orientations of individual faults and inherent striations, combined with the sense of slip on each fault. In the Langøy-Algrøy area, the sense of slip was estimated from the offset of gneiss banding and the geometry and arrangement of steps along the fault surfaces (e.g. Petit 1987).

Separating fault-slip data related to different deformation phases and stress fields is another fundamental principle in kinematic analyses. As argued above, the structural evolution in the study area was polyphase. Thus, care should be taken when analyzing the striated faults. The formation of these faults apparently relates to at least two main deformation phases, and a mean to separate the data is provided by the established relationship between epidote and calcite precipitation. This relationship indicates that most set II faults were not formed, or were at least not active at the time of epidote precipitation. Allowing only these faults to be analyzed (i.e. NNE-SSW to NW-SE trending faults without epidote) would therefore reduce the chance of interference with the earlier set I faults, although some overlapping may occur. In contrast, set I faults reflect more than one deformation phase. The striation at some of these faults clearly formed during the epidote precipitation, i.e. during the earliest brittle deformation phase. Other fault surfaces exhibit two striation trends, indicating that they were active at least twice. Some striated faults, however, are not mineralized at all, meaning that the striation could be related to any deformation phase. In

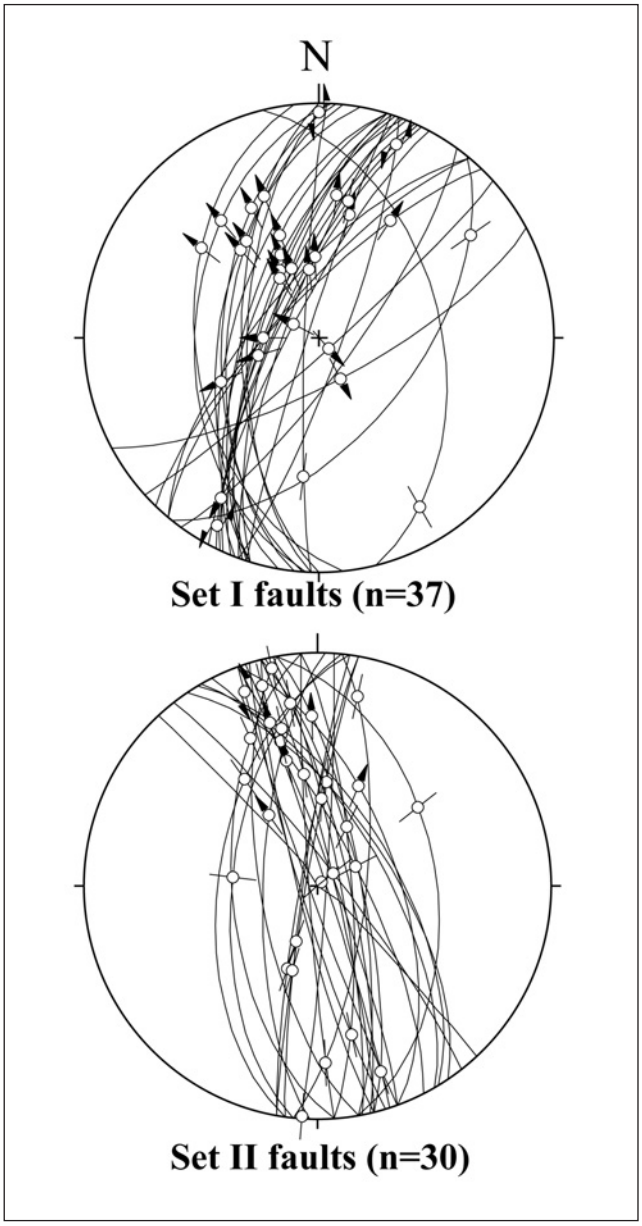

Fig. 8. Stereoplots (equal area lower hemisphere projections) of striated set I and II faults.

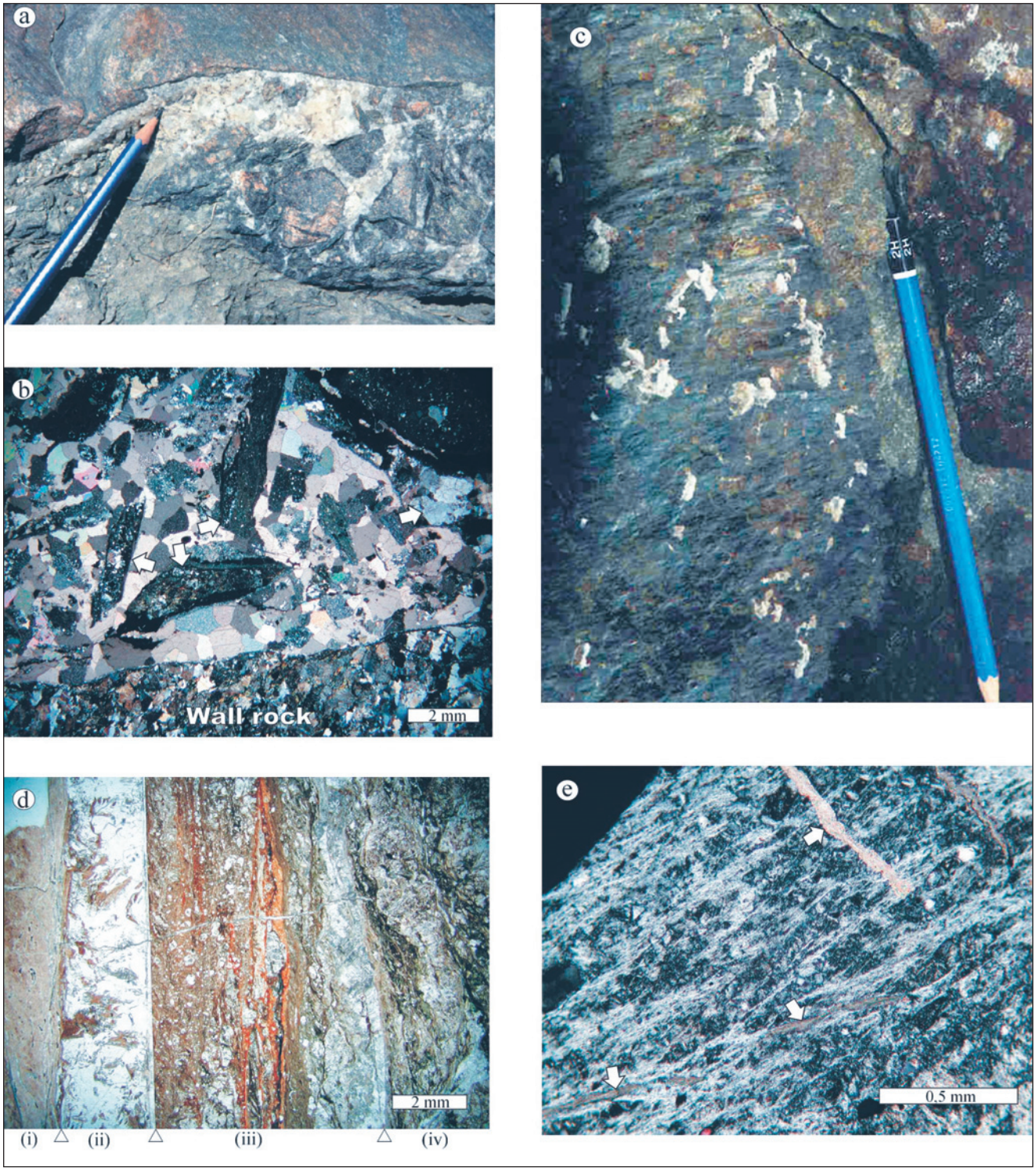

Fig. 9. (a) Set II hydraulic breccia vein with angular fragments "floating" in a matrix of hydrothermal calcite. (b). Microphotograph (crossed polars) of two types of breccia fragments within the calcite fill, one derived from the quartz-feltspatic wall rock (arrow to the right) and the other from a ultracataclasite (arrows to the left). (c) Set II fault with sub-horizontal striation developed in calcite. Steps in the mineralization indicate sinistral displacement, in agreement with the right-stepping en-echelon geometry associated with the fracture (not shown on the picture). (d) Microphotograph (plane polarized light) of slickensided set II fault reflecting several deformational and mineral depositional events (mostly calcite) along distinct zones (i-iv): (i) The slickenside surface is comprised of foliated ultracataclasite, dominated by very fine-grained quartz with minor calcite (see also Fig. 9e). (ii) Coarse-grained calcite, weakly overprinted by the slickenside zone (i). (iii) Cataclasite with alternating foliated and random fabric. Hydrothermal calcite in this zone is strongly overprinted by these fabrics. (iv) Proto-cataclasite with calcite matrix. The latest generation of calcite occurs in veins that crosscut the zones described above. (e) Microphotograph (crossed polars) showing foliated fabric defined by anastomosing shear bands and very fine-grained, elongated quartz with strong lattice-preferred orientation (seen with gypsum plate inserted). Later calcite veins reactivate and cut this fabric (arrows). All pictures are from the Langøy-Algrøy area.

order to reduce the chance of interference between different data sets, only those faults with recorded epidote were analyzed. As a consequence, a group of NE-SW trending faults without epidote, which turned out to have a dominant component of strike-slip displacement, were excluded from this set. It is reasonable to incorporate this group of faults with set II, since these are often associated with strike-slip dominated displacement.

Results

Set Ia faults. – Inversion analysis of low-angle faults of set Ia yielded a vertical σ_1 and a WNW-ESE trending σ_3 (Fig. 7). In terms of strain, this result suggests faulting under vertical shortening and WNW-ESE extension.

Set Ib faults. –Most epidote-filled faults are normal with a large dip-slip component. These set Ib faults are consistent with faulting under NW-SE extension and subvertical shortening (Fig. 10b). Many set Ib fractures represent steep, unsheared mode I fractures. Such fractures open perpendicular to their margins, and their general NE-SW to NNE-SSW trend confirms the result of the inversion analysis.

A subordinate group of steep, epidote-filled strike-slip faults appears to have sinistral displacement components. These are locally found together with dip-slip striations, suggesting that the epidote-bearing faults were reactivated under a new stress field. Inversion of these fault data (Fig. 10c) reveals that the data are too few to yield meaningful results. Based on the dominant strike-slip displacement along these faults, it is likely that they kinematically relate to set II faults. Possible set Ib faults without mineralization have been excluded from the paleostress analyses

Set II faults. – Analyzing the striated set II faults in combination with faults extracted from set I (the strike-slip faults shown in Fig. 10c) yielded principle stress axes that are consistent with faulting under E-W extension (Fig. 10d). The same result was obtained when faults extracted from set I were excluded. Most set II fractures are steep hydraulic veins, which opened in the direction of the local σ_3. The general NNW-SSE trend of these veins is therefore in good agreement with the stress inversion results. However, the obliqueness of the principal stress axes deviates from the ideal horizontal and vertical orientations expected from homogeneous data sets (Angelier 1994). This can be an artifact of the limited spread in orientation of the data (the majority of the faults are steep N-S striking faults with considerable strike-slip components), but could also reflect a change in the stress field orientation during the multi-stage evolution of Set II fractures (discussed below).

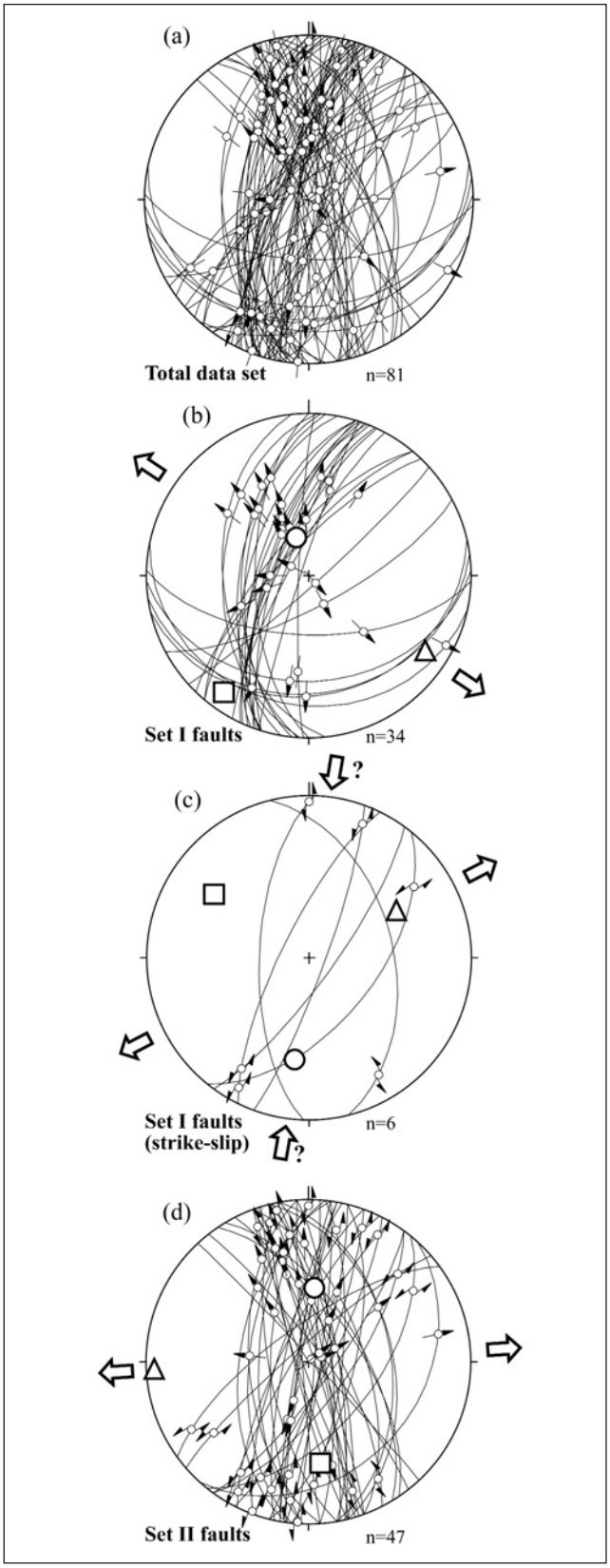

Fig. 10. Stress inversion analyses of fault slip data from the Langøy-Algrøy area. Circles=σ_1, squares=σ_2 and triangles=σ_3. (a) All of the recorded faults with striation. (b) Epidote-filled faults dominated by normal displacement. (c) Epidote-filled faults dominated by strike-slip displacement (sinistral). d) NNE-SSW (010-190) to NW-SE trending set II faults, combined with faults extracted from set I. See text for details.

Geochronology

Analytical methods

Transparent shards of single sphene crystals were washed in distilled water, hot 6N HNO_3 and distilled acetone. The crystal fragments were weighed into a savillex capsule together with a mixed $^{205}Pb/^{235}U$ spike and dissolved in hydrofluoric and nitric acid. U and Pb from the dissolved mineral fractions were eluted in miniaturized anion exchange columns. The isotopic ratios were measured on a Finnigan 262 mass spectrometer housed in the Department of Geology, University of Bergen. The results are listed in Table 2. Error analyses follow the recommendation of Ludwig (1980), and the decay constants used for calculating the ages are taken from Steiger and Jäger (1977).

Epidote and K-feldspar fragments were washed in distilled water, weighed into savillex capsules and dissolved in a mixture of HF and HNO_3. The dissolved samples were split and a mixed $^{87}Rb/^{84}Sr$ spike was added to one half of the split samples. Sr and Rb were separated by specific extraction chromatography using the method described by Pin et al. (1994). Sr and Rb were loaded on double filaments and analyzed in static mode on a Finnigan 262 mass spectrometer. The results of these analyses and the isotope dilution calculations are listed in Table 3.

Sampling and field relations

U/Pb analyses. – Sphene crystals with well-developed morphologies are occasionally intergrown with the minerals typically found in set I fractures, i.e. epidote, quartz and chlorite (Fig. 6a). It therefore appears that the sphene crystallized during the earliest brittle deformation phase in the ØC, based on the relationships between fracture mineralization and fracturing documented above.

For the purpose of U/Pb dating, samples of sphene (SP1 and SP2) were collected from two fractures in the Toftøy and Turøy area, some 15 km north of the main study area (Fig. 1). In general, the overall pattern of brittle structures in this area is dominated by NE-SW and NNW-SSE trending fractures, in which the former fractures typically contain epidote (Bernhard 1994; Grünwald 1994; Ytredal 1995). This pattern is consistent with the Langøy-Algrøy area, suggesting that the fracture development in the two areas was similar.

Sample SP1 (Toftøy, UTM KN 777106) was collected from a releasing step of a mesoscale striated normal fault dipping 50° WNW. This fault cuts ductile top-to-the-W fabric in the surrounding gneiss described by Rykkelid & Fossen (1992) and formed in relation to steeper, NE-SW trending extensional veins at the same outcrop. Epidote, quartz and chlorite are common in these extensional veins, but also occur in deformed (polished) states along the sampled fault.

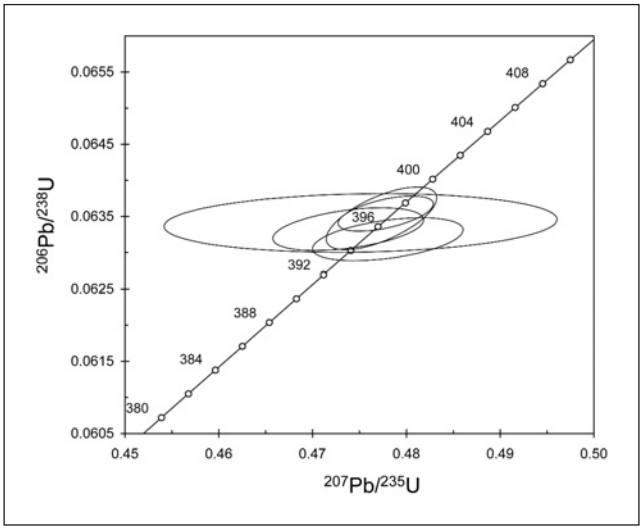

Fig. 11. U/Pb concordia diagram of sphenes in set I fractures (see text for details).

Sample SP2 (Turøy, UTM KN 757092) was sampled from a several centimeter thick extensional vein with euhedral, coarse-grained quartz and epidote. This vein cuts a weakly deformed amphibolite and continues into the surrounding gneiss where it cuts the ductile fabric. The vein dips 50° NW.

In addition to the samples described above, a sample of sphene (SP3) was collected from a NE-SW trending fracture with chlorite on Toska (Fig. 1). The island of Toska occupies a position within the Caledonian allochthons of the Bergen Arc System. Although no detailed field relations of this fracture have been established, the orientation and mineral fill tentatively relate the fracture to set I fractures in the ØC.

Rb/Sr analyses. – Throughout most of the ØC, hydrothermal wall rock alteration is a characteristic feature along roughly NE-SW trending, epidote-mineralized fractures (set I). Alkali-feldspar in the Precambrian wall rock close to these fractures is clearly affected by this alteration (see above), suggesting that these minerals may have been open for isotopic exchange during the circulation of hot fluids. If correct, the alkali-feldspar in the altered wall rock and the hydrothermal epidote (post-Caledonian) may be suitable for Rb/Sr dating. Epidote and altered alkali-feldspar pairs were thus sampled from set I fractures in the Turøy area (EP1 and EP2) and Langøy-Algrøy area (EP3) for Rb/Sr two-point isochron dating.

Sample EP1 (road to Turøy, UTM KN 767098) was collected from a striated set I-fault (Fig. 6b) from a wide fault zone with abundant epidote mineralization.

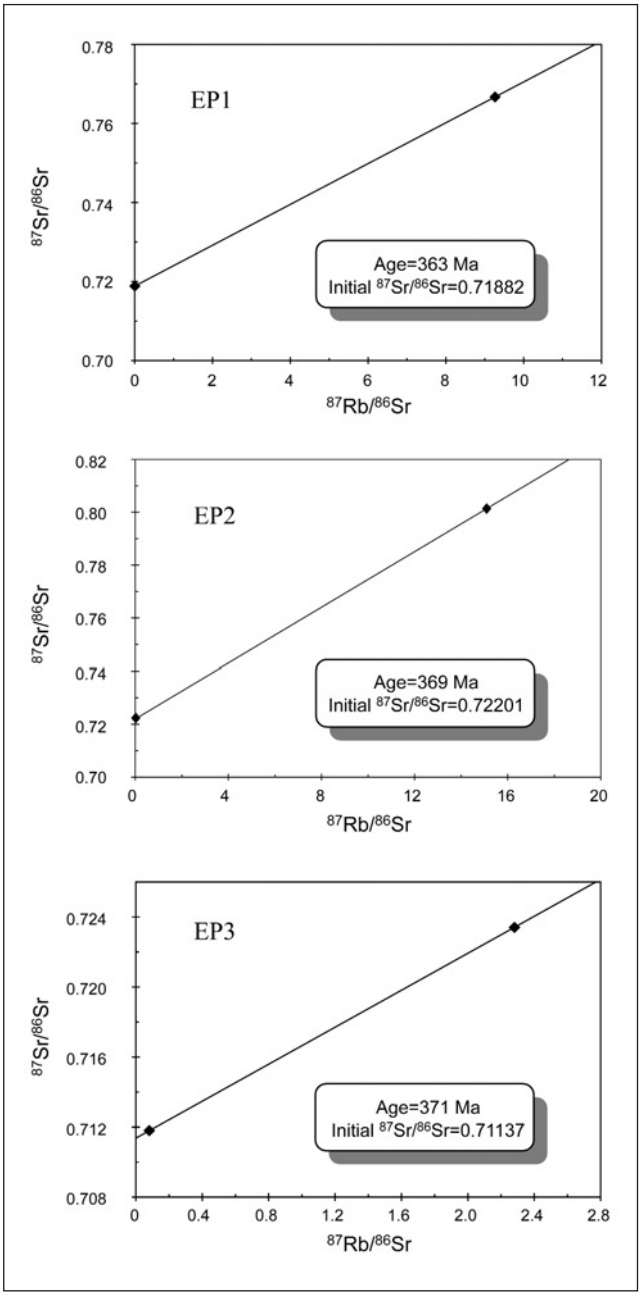

Fig. 12. Rb/Sr two-point isochrons of epidote and alkali-feldspar related to set I fractures (see texts for details).

Multiple kinematic indicators along this fault zone are consistent with NW-SE extension and vertical shortening (Bernhard 1994; Fossen 1998). In thin section, the sample shows evidence of cataclastic deformation, and the crushed epidote along the fault is very fine-grained (Fig. 6c). Thus, the sample conforms kinematically and mineralogically with striated set I faults in the Langøy-Algrøy area.

Sample EP2 (Turøy, UTM KN 758091) was taken from a NE-SW trending extensional vein. In addition to euhedral and coarse-grained epidote and quartz, this vein contains accessory amounts of sphene, thus resembling the fracture from which sample SP2 was collected (above).

Sample EP3 (Langøy-Algrøy area, UTM KM 789977) is from a steep, NNE-SSW trending extensional vein with relatively coarse-grained epidote and quartz as the major mineral fill.

Results

U/Pb analyses of sphene contained in set I fractures yielded Early Devonian ages ranging from 399-393 Ma ($^{206}Pb/^{238}U$ ages including 2σ errors), with a mean of 396 Ma (Table 2 & Fig. 11). The Early Devonian age is interpreted to date sphene growth in association with precipitation of hydrothermal epidote (± quartz ± chlorite). Thus, the documented relationship between mineral precipitation and set I fracture formation (above) suggests that this age dates the onset of the post-Caledonian brittle deformation in the Bergen Arc System.

Rb/Sr two-point isochron dating of epidote and alkali-feldspar yielded fairly consistent Middle-Late Devonian ages of 363 Ma, 369 Ma and 371 Ma (Table 3 & Fig. 12). The dated samples show clear evidence of hydrothermal alteration of the wall rock, thus, these ages are probably influenced by infiltration of hot fluids during or after set I fracturing. None of the dated samples appears to be associated with reactivation and precipitation of calcite, as judged by thin section studies, suggesting that the Rb/Sr system may have been closed during precipitation of calcite in the set II fractures.

Discussion

Devonian cooling history and the onset of post-Caledonian brittle deformation

Based on the new radiometric ages presented above and previous radiometric ages, it is argued that the onset of brittle deformation in the ØC occurred at around 396 Ma. $^{40}Ar/^{39}Ar$ ages of amphibole and biotite indicate cooling from 550-500°C to 300-350°C within the 410-400 Ma period (Boundy et al. 1996; Fossen & Dunlap 1998), implying a cooling rate of 15-20°C/my (Fig. 13). With a thermal gradient of 25°C/km, this cooling rate corresponds to an exhumation rate of 0.6-0.8 mm/y. The new data thus indicate that rocks of the ØC cooled from amphibolite facies conditions into the brittle regime (<300°C) at 396 Ma.

Near the end of the Caledonian contractional history, high-pressure estimates in the basement region of SW Norway (the WGR and ØC) indicate a subduction setting with the northwesternmost part of the basement dipping as steep as 45° NW (Fossen 2000 and references

Table 2. U/Pb data of sphenes in fractures from the Bergen Arc System

Fractions			Concentration		Measured		Atomic ratios[b]							Ages					
Sample	Properties	Weight (mg)	U (ppm)	Pb_{rad} (ppm)	Pb_{com} (pg)	$^{206}Pb/^{204}Pb$[a]	$^{208}Pb/^{206}Pb$	$^{206}Pb/^{238}U$	± (2σ)	$^{207}Pb/^{235}U$	± (2σ)	$^{207}Pb/^{206}Pb$	± (2σ)	$^{206}Pb/^{238}U$	± (2σ)	$^{207}Pb/^{235}U$	± (2σ)	$^{207}Pb/^{206}Pb$	± (2σ)
SP1a	Brown fragm.	0.434	0.104	0.008	679	275	0.1574	0.06347	36	0.4774	48	0.05456	42	396.7	2.2	396.3	3.3	394.2	17.2
SP1b (1)	Brown fragm.	0.501	0.112	0.008	848	277	0.1527	0.06354	20	0.4779	1	0.05455	40	397.1	1.2	396.6	2.8	393.7	16.7
SP1b (2)	Brown fragm.	0.501	0.112	0.008	849	276	0.1527	0.06344	23	0.4784	44	0.05469	42	396.5	1.4	396.9	3.0	399.6	17.5
SP2 (1)	Yellow fragm.	0.890	0.067	0.007	1691	157	0.6391	0.06332	24	0.4739	65	0.05428	68	395.8	1.5	393.9	4.5	382.9	28.4
SP2 (2)	Yellow fragm.	0.890	0.067	0.007	1685	157	0.6386	0.06318	24	0.4781	65	0.05488	68	394.9	1.5	396.8	4.5	407.5	28.0
SP3	Yellow fragm.	1.403	0.040	0.006	2572	104	1.0217	0.06341	33	0.4752	170	0.05436	193	396.3	2.0	394.8	11.8	386.0	81.3

a) Corrected for fractionation.
b) Corrected for fractionation and spike, 30 pg Pb blank and initial common lead calculated from Stacey and Kramers (1975) and 2 pg U blank.
The analyses were run twice on the samples SP1b and SP2.

herein). It appears from $^{40}Ar/^{39}Ar$ mica ages that deformation under the Jotun Nappe, much closer to the foreland in the east, was still ductile at around 400 Ma (Fossen & Dunlap 1998). The similar $^{40}Ar/^{39}Ar$ mica cooling ages obtained in the hinterland (referred to above) indicate that the westerly dip of the basement between the ØC and the foreland was more or less removed through differential uplift at around 400 Ma. The onset of brittle deformation at 396 Ma in the ØC further emphasizes how extension-driven uplift and cooling continued after 400 Ma. U-Pb ages from the northwestern, ultra-high pressure part of the WGR (Fig. 1, inset) indicate that this portion of the basement was still at 30-40 km depth at 395 Ma (Terry et al. 2000), but that exhumation was going on at a higher rate than in the ØC.

Age of macroscopic folding

Constraining the onset of brittle deformation in the ØC to the Early Devonian implies that the formation of large-scale E-W trending folds in the ØC (Fig. 1) is no younger than Early Devonian in age. The possibility that these folds are products of the late Devonian to early Carboniferous N-S shortening that affected the Middle Devonian basins to the north (Chauvet & Séranne 1994; Hartz & Andresen 1997; Osmundsen et al. 1998; Braathen 1999; Larsen 2002) is therefore unlikely. This phase of N-S shortening and accompanying E-W extension may, however, have generated or reactivated faults (hidden in the set II data?) in the ØC.

Table 3. Rb/Sr data of fracture mineral fill in the ØC

Sample	Rb (ppm)	Sr (ppm)	$^{87}Rb/^{86}Sr$	$^{87}Sr/^{86}Sr$	2σ
EP1					
Epidote	81,37322	2894,597	0,081368	0,711799	9,2E-06
K-feldspar	133,4945	169,6367	2,280474	0,72341	9,5E-06
EP2					
Epidote	19,20992	2326,081	0,023929	0,722137	8,6E-06
K-feldspar	287,9108	55,91928	15,09452	0,801384	9,4E-06
EP3					
Epidote	4,143788	4950,104	0,002425	0,718841	9,0E-06
K-feldspar	284,0122	89,25024	9,263024	0,766715	9,1E-06

Implication of the Rb/Sr ages and the duration of Devonian Set I faulting

Whereas the U-Pb ages are confidently interpreted as the age of crystallization of sphene, the roughly 30 m.y. younger Rb/Sr isochron ages of epidote and alkali-feldspar are more difficult to interpret. More so than the U-Pb system, the Rb/Sr system is prone to have been affected by hydrothermal activity along the set I fracture system. The fact that such activity has occurred is evident from the characteristic alkali-feldspar alteration around the Set I fractures. Such pulses are typically related to periods of faulting or opening of the fractures, and as such related to periods of increased tectonic stress and fault activation. The Rb/Sr ages are Late Devonian, and one could speculate that the faulting is connected with syn- to post-depositional faulting in the mid-Devonian basins and their substrate to the north of the study area (Hartz & Andresen 1997; Osmundsen et al. 1998). However, additional data are required for a closer assessment of these ages.

The NW-SE directed extension revealed by set I faults in the ØC is consistent with other paleostress/strain calculations from southwestern Norway (Seranne & Seguret 1987; Fossen 1995, 2000; Valle et al. 2002). The ~396 Ma age of sphene from these faults indicates their initiation in the Early Devonian, and the cohesive nature of the fault rocks and association with ductile

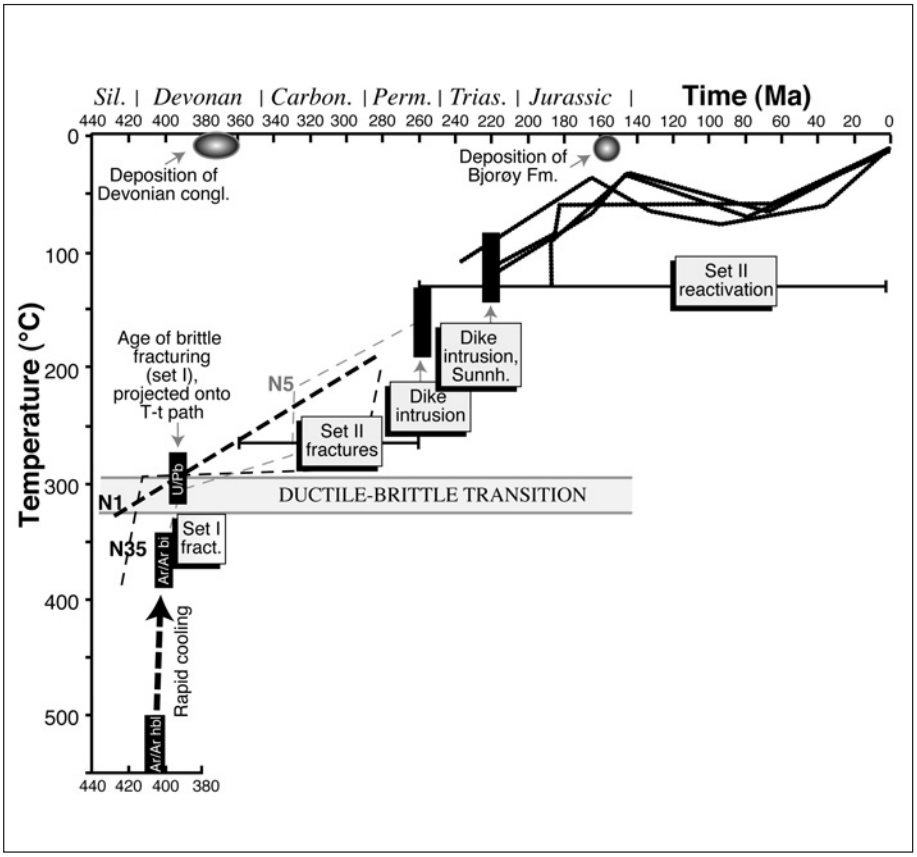

Fig. 13. Temperature-time diagram with age constraints from this study combined with the post-Scandian cooling path for the Caledonian hinterland in the Bergen area and southwards: $^{40}Ar/^{39}Ar$ hornblende and biotite ages (Fossen & Dunlap 1998) and U/Pb ages of sphene (this study) indicate rapid cooling and uplift in the Early Devonian. Semi-brittle to brittle set I fractures in the ØC related to this phase were apparently active through much of the Devonian period. Further cooling of the crust to temperatures around 100-150°C in the Permo-Triassic is based on K-feldspar $^{40}Ar/^{39}Ar$ thermochronology (sample numbering according to Dunlap & Fossen 1998), K-Ar dating of dikes in the ØC (~260 Ma, Løvlie & Mitchell 1982) and $^{40}Ar/^{39}Ar$ dating of more southerly dikes (~220 Ma, Fossen & Dunlap 1999). Set II fractures in the ØC evolved through several stages during this period until the emplacement of Permian dikes. Later reactivations of set II fractures occurred at shallow crustal levels, as indicated by apatite fission track analyses (Fossen, Gabrielsen & Andriessen, unpubl. data).

deformation components (set Ia) indicate deep burial (~10 km). However, fracture systems consistent with NW-SE extension are also found to affect Middle Devonian sediments to the north of the ØC, notably the Solund basin (Seranne & Seguret 1987), the Kvamshesten basin (Osmundsen et al. 1998), and their substrate (Chauvet & Séranne 1994), indicating NW-SE extension during and after the formation of the Middle Devonian basins. Furthermore, veins in the Hornelen Basin indicate NW-SE extension (Odling & Larsen 2000), and Rb/Sr ages related to set I fractures presented in this work are Late Devonian. Collectively, these observations suggest that the extensional strain field responsible for set I fractures may have persisted throughout much of the Devonian time period since ~396 Ma.

The transition from NW-SE to E-W extension (Set I to Set II fractures)

Set II fractures are demonstrably younger than set I fractures and they indicate E-W extension, i.e. different from the NW-SE extension recorded by set I fractures. A similar change in the extension direction is inferred from study of veins in the Hornelen basin (Odling & Larsen 2000). The change from NW-SE to E-W extension is, however, not very well defined in time. Permian (260 Ma) dikes intruding some of the set II fractures provide a minimum age for the onset of E-W extension (Fossen 1998; Valle et al. 2002). E-W extension at this time is well known and responsible for early rift formation in the North Sea (e.g. Gabrielsen et al. 1990), formation of the Oslo Rift (Ramberg & Larsen 1978; Heeremans et al. 1996), and numerous coast-parallel dikes in SW Norway (Færseth et al. 1976; Torsvik et al. 1997; Fossen & Dunlap 1999). Permian ages are also obtained from major fault zones in SW Norway (the Lærdal-Gjende fault; Andersen et al. 1999, and the Dalsfjord Fault; Eide et al. 1999). Hence, fracture formation and/or reactivation in the ØC during Permian times is very likely.

There are, however, indications that set II fractures in the ØC may have started to form at an earlier stage. First, a small number of epidote-filled fractures ascribed to set I seems to be kinematically related to set II, suggesting that epidote was still forming at the beginning of the second extensional phase. Second, possible crystal-plastic deformation of quartz in some early set II faults suggests relatively high temperatures at depths close to the ductile-brittle transition. Considering the cooling path indicated by alkali-feldspar thermochronology (Dunlap & Fossen 1998) (Fig. 13), this observation indicates that set II fractures started to form in the latest Devonian or Carboniferous. During intrusion of dikes along the set II fractures in the Permian, a likely temperature of ~150°C was suggested by Løvlie & Mitchell (1982). This is in agreement with alkali-feldspar thermochronology (Fig. 13), implying that the ØC at that time (260 Ma) was situated at a crustal depth in

the order of 5 km. Hence, it can be inferred that the initiation of set II fractures closely followed the latest stages of set I fracture formation, possibly around the Devonian-Carboniferous transition. The formation of striated set II faults, of which remnants are found in later breccia veins, is thought to be mostly restricted to this initial stage. Hydraulic fracturing and the formation of calcite-filled breccia veins at decreasingly shallower crustal levels dominated further development of set II fractures, until the Permian dikes intruded. This multistage development apparently resulted in a mix of set II fractures related to Late Devonian to Early Carboniferous N-S shortening/E-W extension followed by Permian vertical shortening/E-W extension, in agreement with the kinematic analyses presented above.

E-W extension throughout the Mesozoic?

E-W extension is thought to have persisted throughout the Permian, Triassic and Jurassic in the offshore area west of Bergen, while the fault activity tapered off into the Cretaceous (Gabrielsen et al. 1990; Roberts et al. 1990; Færseth et al. 1997). The evidence for fault reactivation at shallow crustal levels (non-cohesive fault products) is mainly from N-S to NNW-SSE trending fractures and lineaments, indicating that this extensional strain field also affected the coastal areas. Significant reactivation of the Hjeltefjord fault zone after the deposition of the Bjorøy Formation and time-equivalent sediments offshore (Fossen et al. 1997) is likely to be of latest Jurassic-early Cretaceous age – a tectonically active time period in the offshore area (op. cit.). However, even later reworking is clearly possible, as current earthquake activity and neotectonics are reported in coastal areas of southwest Norway and in the North Sea (e.g. Hicks et al. 2000).

Conclusion

Two main sets of semi-brittle to brittle fractures, corresponding to at least two main extensional phases have been identified. The earliest phase involved the formation of set I fractures during NW-SE extension and precipitation of mainly epidote, quartz and chlorite. The later extensional deformation caused reactivation of these fractures and the formation of set II fractures along with hydrothermal precipitation of calcite. The age of the epidote-bearing set I fractures is constrained by U/Pb dating of sphene (~396 Ma). Somewhat younger Rb/Sr two-point isochron dating of epidote and hydrothermally altered alkali-feldspar in the wall rock (363 Ma, 369 Ma and 371 Ma) is related to subsequent hydrothermal activity along these fractures. Together with regional considerations, these results indicate that NW-SE extension governs much of the Devonian time period from around 396-365 Ma. Early faults in the ØC transect large-scale basement folds, indicating that these folds are older than similar trending folds that affect the Devonian basins to the north (Late Devonian to Early Carboniferous in age).

The change to E-W extension and formation of set II fractures is thought to have occurred shortly after the NW-SE extensional deformation, probably close to the Devonian-Carboniferous boundary or during the Carboniferous. Later E-W extensional reactivation of the fracture systems occurred repeatedly throughout the Mesozoic and probably also later.

Acknowledgments: - This paper is part of the first authors Dr. scient thesis work. Yuval Ronen is thanked for his help with the Rb/Sr analyses. Detailed reviews by Ebbe Hartz and Øystein Nordgulen significantly improved the paper.

References

Andersen, T. B., Torsvik, T.H. Eide, E.A., Osmundsen, P.T. & Faleide, J.I. 1999: Permian and Mesozoic extensional faulting within the Caledonides of central Norway. *Journal of the Geological Society, London 156,* 1073-1080.

Angelier, J. 1984: Tectonic analysis of fault slip data. *Journal of Geophysical Research 89,* B7, 5835-5848.

Angelier, J. 1994: Fault slip Analysis and Palaeostress Reconstruction. *In* Hancock, P. L. (ed.): *Continental Deformation.,* 53-100. Pergamon, Oxford, pp..

Bering, D. H. 1984: *Tektono-metamorf utvikling av det vestlige gneiskompleks i Sund, Sotra.* Cand. real. thesis, University of Bergen.

Bernhard, J. 1994: *Brittle deformation in the Øygarden Gneiss Complex, Western Norway – palaeostress analysis.* Cand. real. thesis, University of Bergen.

Boundy, T. M., Essene, E. J., Hall, C. M., Austrheim, H. & Halliday, A. N. 1996: Rapid exhumation of lower crust during continent-continent collision and late extension: Evidence from $^{40}Ar/^{39}Ar$ incremental heating of hornblendes and muscovites, Caledonian orogen, western Norway. *Geological Society of America Bulletin 108,* 1425-1437.

Braathen, A. 1999: Kinematics of post-Caledonian polyphase brittle faulting in the Sunnfjord region, western Norway. *Tectonophysics 302,* 99-121.

Chauvet, A. & Séranne. M. 1994: Extension-parallel folding in the Scandinavian Caledonides: implications for late-orogenic processes. *Tectonophysics 238,* 31-54.

Deer, W. A., Howie, R. A. & Zussman, J. 1992: The rock forming minerals. 696 pp. John Wiley & Sons, New York.

Eide, E. A., Torsvik, T. H.. Andersen, T. B. & Arnaud, N. O. 1999: Early Carboniferous unroofing in western Norway: A tale of alkali feldspar thermochronology. *The Journal of Geology 107,* 353-374.

Etchecopar, A., Vasseur, G. & Daignieres, M. 1981: An inverse problem in microtectonics for the determination of stress tensors from fault striation analysis. *Journal of Structural Geology 3,* 51-65.

Evans, A. M. 1993: Ore geology and industrial minerals, an introduction. 389 pp. Blackwell Science.

Fossen, H. & Rykkelid, E. 1990: Shear zone structures in the Øygarden area, west Norway. *Tectonophysics 174,* 385-397.

Fossen, H. 1992: The role of extensional tectonics in the Caledonides of south Norway. *Journal of Structural Geology 14,* 1033-1046.

Fossen, H., Mangerud, G., Hesthammer, J., Bugge, T. & Gabrielsen, R. H. 1997: The Bjorøy Formation: a newly discovered occurrence of Jurassic sediments in the Bergen Arc System. *Norsk Geologisk Tidsskrift 77,* 269-287.

Fossen, H. 1998: Advances in the understanding of the post-Caledonian structural evolution of the Bergen area, west Norway. *Norsk Geologisk Tidsskrift 78,* 33-46.

Fossen, H. & Dunlap, W. J. 1998: Timing and kinematics of Caledonian thrusting and extensional collapse, southern Norway: evidence from $^{40}Ar/^{39}Ar$ thermochronology. *Journal of Structural Geology 20,* 765-781.

Fossen, H. & Dunlap, W. J. 1999: On the age and tectonic significance of Permo-Triassic dikes in the Bergen-Sunnhordland region, southwestern Norway. *Norsk Geologisk Tidsskrift 79,* 169-178.

Fossen, H. 2000: Extensional tectonics in the Caledonides: Synorogenic or postorogenic? *Tectonics 19,* 213-224.

Færseth, R. B., Macintyre R. M. & Naterstad, J. 1976: Mesozoic alkaline dykes in the Sunnhordaland region, western Norway, ages, geochemistry, and regional significance. *Lithos 9,* 331-345.

Færseth, R. B. 1978: Mantle-derived lherzolite xenoliths and megacrysts from Permo-Triassic dykes, Sunnhordland, western Norway. *Lithos 11,* 23-35.

Færseth, R. B., Gabrielsen, R. H. & Hurich, C. A. 1995: Influence of basement in structuring of the North Sea basin, offshore southwest Norway. *Norsk Geologisk Tidsskrift 75,* 105-119.

Færseth, R. B., Knudsen, B. -E., Liljedahl, P. S. & Søderstrøm, B. 1997: Oblique rifting and sequential faulting in the Jurassic development of the northern North Sea. *Journal of Structural Geology 19,* 1285-1302.

Gabrielsen et al 1990: Architectural styles of basin fill in the northern Viking graben. *In* Blundell, G. D. & Gibbs, A. D. (eds.): *Tectonic evolution of the North Sea Rifts, 158-179.* Clarendon Press, Oxford.

Grünwald, R. 1994: *Faulted basement in westernmost on-shore Norway (Øygarden) and its off-shore seismic image.* Cand. real. thesis, University of Bergen.

Hartz, E. & Andresen, A. 1997: From collision to collapse: Complex strain permutations in the hinterland of the Scandinavian Caledonides. *Journal of Geophysical Research 102,* B11, 24697-24711.

Heeremans, M., Larsen, B. T. & Stel, H. 1996: Paleostress reconstruction from kinematic indicators in the Oslo Graben, southern Norway: new constraints on the mode of rifting. *Tectonophysics 266,* 55-79.

Hicks, E. C., Bungum, H. & Lindholm, C. D. 2000: Stress inversion of earthquake focal mechanism solutions from onshore and offshore Norway. *Norsk Geologisk Tidsskrift 80,* 235-251.

Johns, C. C. 1981: *The geology of northern Sotra; Precambrian gneisses west of the Bergen Arcs, Norway.* PhD thesis, Bedford College, University of London.

Kolderup, C. F. & Kolderup, N. H. 1940: The Geology of the Bergen Arc System. Bergen Museums Skrifter 20, 1-137.

Larsen, Ø. 1996: Fedjedomens tektoniske utvikling (Øygarden gneiskompleks, vest Norge) – en alternative model for dannelse av gneisdomer. Cand. real. thesis, University of Bergen.

Larsen, Ø. 2002: Kinematics and timing of late- to post-Caledonian deformation in the hinterland region of the Scandinavian Caledonides, with emphasis on the extensional history in SW Norway. PhD thesis, University of Bergen.

Ludwig, K. R. 1980: Calculation of uncertainties of U-Pb isotope data. E*arth Planetary Science Letters 46,* 212-220.

Løvlie, R. & Mitchell, J. G. 1982: Complete remagnetization of some Permian dykes from western Norway induced during burial/uplift. *Physics of the Earth and Planetary Interiors 30,* 415-421.

Milnes, A. G. & Wennberg, O. P. 1997: Tektonisk utvikling av Bergensområdet. *Geonytt 1,* 6-9.

Odling, N. & Larsen, Ø. 2000: Vein architecture in the Devonian sandstones of the Hornelen basin, western Norway, and implications for the palaeostrain history. *Norsk Geologisk Tidsskrift 80,* 289-299.

Osmundsen, P. T., Andersen, T. B., Markussen, S. & Svendby, A. K. 1998: Tectonics and sedimentation in the hangingwall of a major extensional detachment: the Devonian Kvamshesten Basin, western Norway. *Basin Research 10,* 213-234.

Passchier, C. W. & R. Trouw, A. J. 1996: *Microtectonics.* 289 pp. Springer-Verlag.

Petit, J.P. 1987: Criteria for the sense of movement on fault surfaces in brittle rocks. *Journal of Structural Geology 9,* 597-608.

Phillips, W. J. 1972: Hydraulic fracturing and mineralization. *Journal of the Geological Society, London 128,* 337-359.

Pin, C., Briot, D., Bassin, D. & Poitrasson, F. 1994: Concomitant separation of strontium and samarium neodymium for isotopic analysis in silicate samples, based on specific extraction chromatography. *Analytica Chimica Acta 298,* 209-217.

Ramberg, I. B. & Larsen, B. T. 1978: Tectonomagmatic evolution. In: Dons, J. A. & Larsen, B. T. (eds.): The Oslo Paleorift: a review and Guide to Excursions. *Norges Geologiske Undersøkelse 337,* 55-73.

Roberts, A. M., Yielding, G. & Badley, M. E. 1990: A kinematic model for the orthogonal opening of the late Jurassic North Sea rift system, Denmark-Mid Norway. *In* Blundell, G. D. & Gibbs, A. D. (eds.): *Tectonic evolution of the North Sea Rifts,* 180-199. Clarendon Press, Oxford.

Rykkelid, E. & Fossen, H. 1992: Composite fabric in mid-crustal gneisses: observations from the Øygarden Complex, West Norway Caledonides. *Journal of Structural Geology 14,* 1-9.

Seranne, M. & Seguret, M. 1987: The Devonian basins of western Norway: tectonics and kinematics of an extending crust. *Geological Society of London Special Publication 28,* 537-548.

Stacey, J. S. & Kramer, J. D. 1975: Approximation of terrestrial lead isotope evolution by a two-stage model. *Earth and Planetary Science Letters 26,* 207-221.

Steel, R.J., Siedlecka, A. & Roberts, D. 1985: The Old Red Sandstone basins of Norway and their deformation: a review. *In* Gee, D.G. & Sturt, B.A. (eds.): *The Caledonide Orogen-Scandinavia and related areas,* 293-315. Wiley, Chichester.

Steiger, R.H, and Jäger, E. 1977: Subcommission on Geochronology: Convention on the use of decay constants in geo- and cosmochronology. *Earth Planetary Science Letters 36,* 359-362.

Sturt, B. A., Skarpenes, O., Ahanian, A. T. & Pringle, I. R. 1975: Reconnaissance Rb/Sr isochron study in the Bergen Arc System and regional implications. *Nature 253,* 595-599.

Sturt, B. A. Thon, A. 1978: Caledonides of southern Norway. In IGCP Project 27, Caledonian-Appalachian orogen of the Atlantic region. *Geological Survey of Canada, Paper 78-13,* 39-47.

Terry, M. P., Robinson, P., Hamilton, M. A. & Jercinovic, M. J. 2000: Monazite geochronology of UHP and HP metamorphism, deformation, and exhumation, Nordøyane, Western Gneiss Region, Norway. *American Mineralogist 85,* 1651-1664.

Torsvik, T. H., Andersen, T. B., Eide, E. A. & Walderhaug, H. J. 1997: The age and significance of dolerite dykes in western Norway. *Journal of the Geological Society, London 154,* 961-973.

Ytredal, T.-O. 1995: *General geology and analysis of brittle structures in the Kollsnes area, Øygarden, western Norway.* Cand. real. thesis, University of Bergen.

Valle, P., Færseth, R. B. & Fossen, H. 2002: Devonian-Triassic brittle deformation based on dyke geometry and fault kinematics in the Sunnhordland region, SW Norway. *Norsk Geologisk Tidsskrift 82,* 3-17.

Wennberg, O. P. & Milnes, A. G. 1994: Interpretation of kinematic indicators along the northeastern margin of the Bergen Arc System: a preliminary field study. *Norsk Geologisk Tidsskrift 74,* 166-173.

Wennberg, O. P., Milnes, A. G. & Winsvold, I. 1998: The northern Bergen Arc Shear Zone – an oblique-lateral ramp in the Devonian extensional detachment system of western Norway. *Norsk Geologisk Tidsskrift 78,* 169-184.